applied sciences

MDPI

Article

Numerical Simulations of Flow and Heat Exchange in Zigzag-Shaped Microchannels

Maciej Staszak and Grzegorz Musielak *

Division of Process Engineering, Institute of Chemical Technology and Engineering, Poznan University of Technology, ul. Berdychowo 4, 60-965 Poznań, Poland; maciej.staszak@put.poznan.pl
* Correspondence: grzegorz.musielak@put.poznan.pl

Featured Application: The results of the work may be used in the design of cooling systems for electronic components.

Abstract: Cooling of electronic components is of great importance currently. One of the most important methods of integrated circuit cooling is the use of microchannel heat sinks. The aim of this work is to analyze the cooling capacity of zigzag shaped microchannels. The heat exchange for four different microchannels was tested depending on the flow rate of the cooling liquid (water) and the temperature of the cooled element. The system of differential equations that describe fluid flow and heat transport is presented in the paper. The equations were solved using the finite volume method. The work showed that both the increase in the number of zigzag sections and the increase in the flow velocity cause an increase in the flow resistance. In contrast, an increase in the temperature of the cooled element causes a decrease in fluid viscosity, which results in a decrease in flow resistance. From the point of heat exchange, both the increase in the number of segments, the flow rate, and the temperature of the cooled element increase the cooling capacity of the microchannel. Research shows that zigzag shaped microchannels are excellent cooling elements, especially for geometrically small heat sources such as electronic components.

Keywords: heat transfer; cooling; convection; microchannel; zigzag shaped; laminar flow

check for updates

Citation: Staszak, M.; Musielak, G. Numerical Simulations of Flow and Heat Exchange in Zigzag-Shaped Microchannels. *Appl. Sci.* **2024**, *14*, 9826. https://doi.org/10.3390/app14219826

Academic Editor: Adrian Irimescu

Received: 1 October 2024
Revised: 18 October 2024
Accepted: 23 October 2024
Published: 28 October 2024

Copyright: © 2024 by the authors. Licensee MDPI, Basel, Switzerland. This article is an open access article distributed under the terms and conditions of the Creative Commons Attribution (CC BY) license (https://creativecommons.org/licenses/by/4.0/).

1. Introduction

The cooling of electronics, in particular integrated circuits, has recently become of particular importance [1]. Currently produced electronic devices move towards miniaturization. At the same time, the number of transistors placed in integrated circuits is constantly growing. This means an increase in thermal power and an increase in heat flux density [2]. As a result, the excessive temperature of electronic devices is the main cause of their failure. It is estimated that up to 55% of electronic device failures are caused by this [3]. This makes it necessary to use more and more efficient cooling systems for integrated circuits. In this way, the performance and reliability of electronic devices can be improved.

Typically, cooling methods are divided into active and passive [1]. Passive systems basically use natural convection, whereas active cooling systems use forced convection. Therefore, active systems must be supplied with external energy to increase the heat dissipation capacity. Of course, active cooling systems generally perform better. According to [4], free convection cooling systems can be used for heat flux densities up to 1.5×10^3 W/m^2, forced air convection up to 1.5×10^4 W/m^2, and forced liquid convection up to 1.0×10^6 W/m^2. Therefore, most methods of cooling high-power electronic devices are developed based on active cooling.

Another division of cooling methods is based on the contact of electronics with the coolant into methods with direct and indirect contact [1]. The simplest direct contact

method is air cooling. It is used to cool low-power electronics [5]. Liquid may be used instead of air. In this case, the cooled electronic device is immersed in a cooling liquid. The method is called immersion cooling. The coolant used in this method should be characterized by good thermal conductivity, high specific heat, and very poor electrical conductivity [6]. Heat exchange can take place by free convection; however, proper forcing of the flow can improve the cooling efficiency by about 50%. The method is widely used to cool servers and data centers.

Another method of direct contact is spray cooling. In this method, the droplets generated in the nozzle are directed to the surface of the cooled element. Droplets in contact with the surface absorb heat from it and evaporate. In this case, the latent heat of the phase change also increases the heat flux discharged from the surface of the cooled element, resulting in very high cooling efficiency [7]. That is why the spray method is one of the most effective cooling methods for high-power electronic devices. The evolution of spray cooling is droplet electrowetting cooling. The main advantages of electrowetting cooling include the fast response, hot spot cooling, and low energy consumption [8]. A method similar to spray cooling is jet impingement cooling. The main difference is that jet impingement cooling does not require droplet atomization [9].

Exemplary methods representing indirect contact coolant with the cooled element are methods using a heat pipe [10] or a vapor chamber [11]. Both methods are based on the use of the latent heat of the phase change. Heat is absorbed from the source, the cooled element, by evaporation of the coolant. Then, the steam is condensed in a condenser acting as a heat sink from which the heat is discharged to the outside. Heat pipes are used for one-dimensional heat transfer, while the evaporation chambers are used for two-dimensional heat transfer [1]. The solid–liquid phase change is also used to cool electronics. PCM (phase-change materials) are usually used in combination with other cooling techniques [12].

A very important method of indirect contact cooling is the use of microchannel heat sinks. This method was proposed by Tuckerman and Pease for the first time in 1981 [13]. The method consists of the flow of the coolant through a series of parallel microchannels [14]. The small cross-section of the channels together with their large number results in a large heat exchange surface. This allows a high value of heat flux density to be handled. In addition, the method allows for good temperature uniformity in the cooling system.

Water was usually used as the coolant. However, the better thermal properties of metal suspensions resulted in a growing interest in their use for heat exchange in microchannels. The disadvantage of this type of suspension is the possibility of channel clogging, as well as the lack of flow stability [14]. Therefore, it was proposed to use nanofluids, i.e., suspensions of solid particles with dimensions of the order of nanometers [15]. Although nanofluids used in the microchannels can improve cooling capacity, after a period of operation, the deposition of nanoparticles leads to clogging of the microchannels, making them ineffective and even damaging electronic devices [1].

A significant part of the research on the use of microchannels for refrigeration is devoted to the shape of the channels. Most of the work concerns rectilinear micro-channels. The simplest solutions are channels with a constant rectangular [13,16], trapezoidal [16,17], triangular [16], or circular cross-section [18]. A comparison between these cross-sections shows better thermal performance of rectangular and circular channels than trapezoidal and triangular ones [16,18].

The second group consists of rectilinear microchannels with a variable cross-section. Various structures are proposed, e.g., alternately converging and diverging microchannels [19] with different ribs [20,21] or fans inside the microchannel [22]. A comprehensive overview of these types of flow structures is provided in [14].

The third group of works is devoted to the study of microchannels with a constant cross-section but non-rectilinear course of the channel. Gaikwad and Nalawade [23] experimentally investigated heat transfer in straight and zigzag-shaped microchannels with water as the cooling fluid. They observed that the heat transfer in zigzag microchannels

increased from 58 to 88% compared to straight channels. At the same time, they observed an increase in pressure drop from 22 to 35% compared to simple microchannels. Sui and coworkers experimentally [24,25] and numerically [26] investigated flow friction and heat transfer in sinusoidal microchannels with a rectangular cross-section. They used water as a coolant. The test results showed that because of efficient mixing in sinusoidal channels, the heat transfer efficiency is much better than in straight channels with the same cross-sections. At the same time, the increase in pressure drop was much smaller than the improvement in heat transfer. Wavy microchannels with a rectangular cross-sections were examined by Sakanova et al. [27]. They analyzed water and three nanofluids as a coolant. In the case of water as coolant, the wavy shape was clearly better. The higher the amplitude and shorter the wavelength of the wave channel, the lower the thermal resistance, especially for higher Reynolds number values. However, when nanofluids were used as coolant, the effect of the wavy channels was unnoticeable and the wavy and straight runs gave very similar cooling efficiency. This means that the use of nanofluids in curved microchannels is not appropriate. Zhou et al. [28] studied numerically the flow of water in similar wavy microchannels with a rectangular cross-section. By optimizing the shape of the microchannel, they achieved a heat transfer improvement of 2.8 times compared to the flow in a straight-line channel for flow with a high Reynolds number. Mohammed et al. [29,30] examined numerically the influence of the microchannel shape on the hydraulic and thermal performance. They analyzed straight, sinusoidal, zigzag, curvy, and step-shaped microchannels. All microchannels had a rectangular cross-section, and water was used as the coolant. The best thermal performance shows a zigzag microchannel. The second place in terms of thermal quality is the curved microchannel, and the third is the sinusoidal one. The step-shaped microchannel does not give much improvement in thermal properties compared to the straight channel. Similar numerical simulations were performed by Parlak [31] for straight, sinusoidal, and zigzag microchannels with a rectangular cross-section. In contrast to [31–33] the results of this work indicate that the sinusoidal shape is better than the zigzag shape. However, in [31], the influence of microchannel walls on heat transfer was not taken into account. Only heat flow in water was considered, assuming thermal insulation on the walls. All authors of numerical simulations assumed a known, constant heat flux supplied to the system [23,29,31]. This allowed determination of the temperature value but did not provide the possibility of determining how microchannels affect the heat flux value.

The main purpose of this work is to check how the temperature of the heat source, the shape of the microchannels, and the fluid velocity affect the heat transfer during cooling. According to [29,30], zigzag-shaped microchannels are chosen. Fluid and heat flows were studied using numerical simulations. As a result of the calculations, it was obtained that with the increase in the flow rate of the coolant and with the increase in the temperature of the heat source, the heat flux discharged with the coolant also increases. Increasing the number of zigzag-shaped segments increases the cooling capacity of the microchannel. This phenomenon is greatest for higher liquid flow velocities.

2. Materials and Methods

The main purpose of this work is to investigate the cooling of electronic components using microchannel heat sinks. Analysis of the available literature [29,30] indicates that the best thermal properties of microchannels with a non-linear course have the zigzag-shaped microchannels. Therefore, heat sinks of this shape are studied in this work. The results of [16,18] show that the rectangular or circular shape of the microchannel cross-section is the best. Since it is difficult to make zigzag-shaped microchannels with a circular cross-section, a rectangular cross-section was chosen for analysis. Such a cross-sectional shape was investigated in works considering microchannels with a non-linear course [24–30].

2.1. Microchannels Geometry

In this work, four types of microchannels were used: a straight channel and three with the angles between each section modified separately. The straight channel was introduced as the element by which the appropriate ranges of flows analyzed in zigzag channels were selected. We established the flow rate for the straight microchannel with a specific objective: to illustrate a scenario where heat removal from the solid surface is not optimized. This baseline scenario was intentionally chosen to highlight a condition that is less than ideal, with discernible room for improvement in heat transfer performance. By doing so, we created a reference point against which the enhancements in heat transfer efficiency, achieved through the introduction of zigzag modifications to the channel geometry, could be quantitatively assessed. Figure 1a presents a dimetric view of the multi-channel shape. Figure 1b presents the details of the single channel with the corresponding sizes used in formulations. The dimensions used in the calculations are given in Table 1.

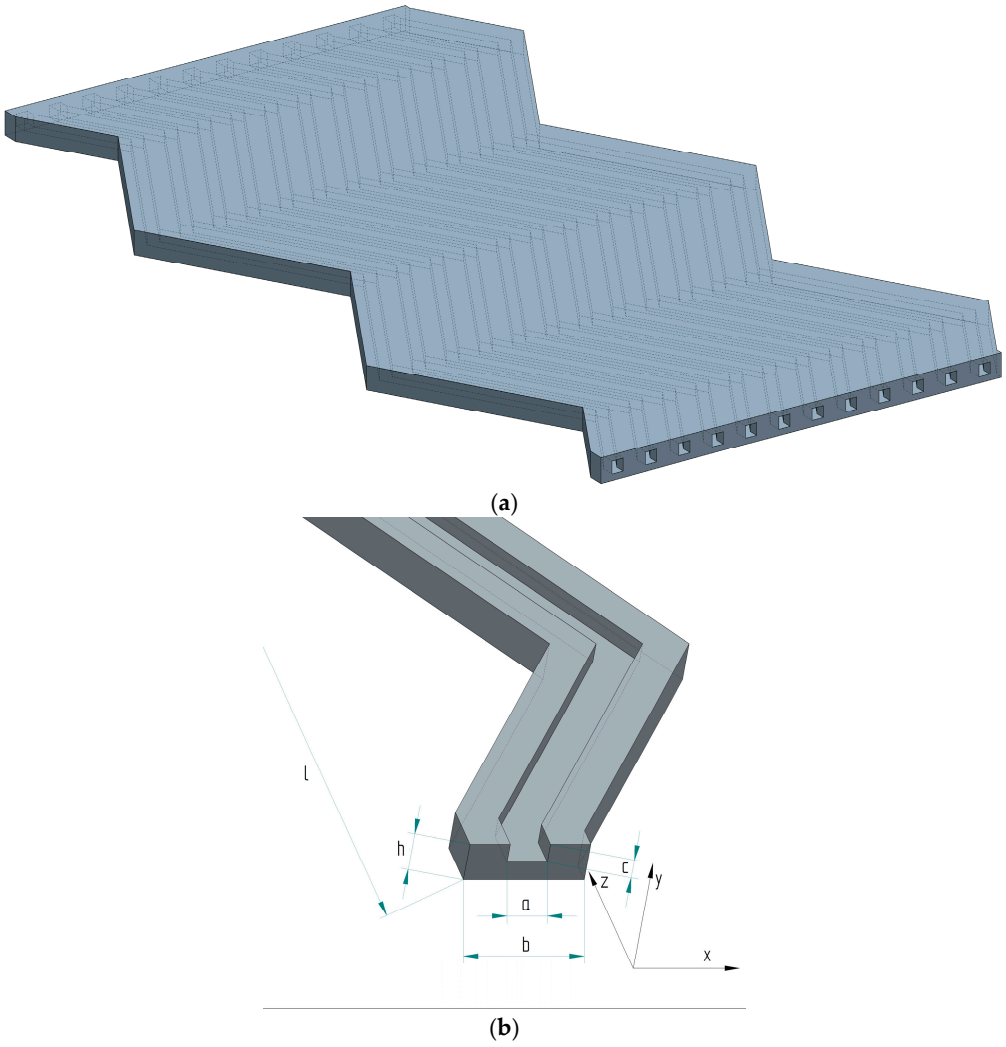


Figure 1. (**a**) Dimetric view of the channels used in simulations. The case presented for zigzag number n = 7. (**b**) Perspective view of the channel inlet/outlet. Dimensions presented are explained in Table 1.

The zigzag profiles were designed using the typical CAD based approach to construct a solid using a leading line. The leading line was formed into a zigzag shape, and the channel solid profile was created by dragging its envelope in a path's preset direction and shape. This ensures that the cross-section always has the specified width.

Table 1. The dimensions used in the calculations.

Dimension (Figure 1b)	Value (mm)
a	1
b	3
c	0.5
h	1
l	80

The process of creating the mesh for the CFD simulations in Ansys Fluent 2022 R1was conducted in accordance with standard procedures, without the use of any special optimization techniques. A tetrahedral mesh was employed for both the flow and solid domains, as this is a common choice due to its flexibility in representing complex geometries. The domains were defined in the SpaceClaim 2022 R1 geometry drawing software, and the same global settings were applied to both domains during the meshing step. The grid element size was determined based on a prior convergence analysis using mass balancing, which ensured adequate model accuracy (Figure in Section 2.4). The interface between the domains was left at the default settings, allowing Fluent to manage the heat exchange automatically.

For all calculated cases, it was assumed that the top and side faces defined symmetry conditions. Inlets to channels were defined by the velocity vector normal to the inlet face, and outlets were defined by a pressure condition specifying the absence of pressure jump at the outlet and, thus, defined free channel discharge. For the sake of graphic clarity, both drawings (Figures 1 and 2) show only the shape of the solid body, while the inner void cavity was also modeled with an appropriately embedded flow space. Interface type conditions were defined between the rigid solid and the body, defining the flow space, which allowed heat transport between the fluid and the solid to be taken into account.

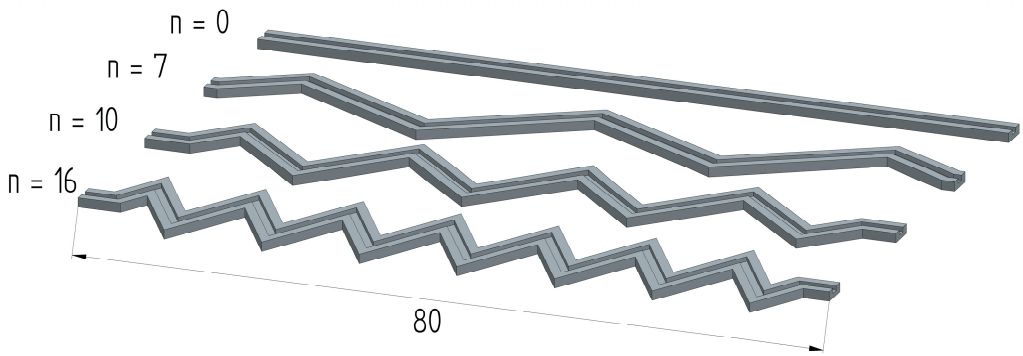


Figure 2. Dimetric view of the four types of channels used.

The bottom face has a temperature boundary condition was defined (see Equation (10)).

2.2. Mathematical Model Assumptions

In order to develop a mathematical model, it is necessary to make appropriate assumptions. These are as follows:

- both the flow of fluid and heat transfer take place under steady state conditions;
- the working fluid is water, which is treated as an incompressible Newtonian fluid;
- fluid flow is caused only by pressure difference, and gravitational force is negligible;
- fluid flow is in a laminar regime;
- thermal expansion of the solid part of the heat exchanger is negligible;
- heat flow in a fluid is caused by convection and conduction;
- the energy dissipation due to viscosity is negligibly small;
- heat flow in a solid is caused by conduction;
- there are no internal heat sources;

- radiation heat transfer is negligible;
- the influence of temperature on fluid density and viscosity is taken into account;
- the specific heat and thermal conductivities of the solid and fluid, and the density of the solid are constant.

Due to the repeatability of identical microchannels (Figure 1), the entire heat exchanger can be divided into repeatable segments. Each segment consists of half of the microchannel and a solid surrounding it (Figure 2). The solid partition between the microchannels is divided into two equal parts belonging to adjacent segments.

2.3. Model Equations

The entire element considered during the calculations can be divided into two regions: a fluid region inside the microchannel and a solid region outside the microchannel.

The phenomena occurring in the fluid region are described by the equations resulting from mass, momentum, and energy balances.

The general form of the fluid flow continuity equation resulting from mass balance is:

$$\frac{\partial \rho_f}{\partial t} + \nabla \cdot \left(\rho_f \vec{v} \right) = 0 \tag{1}$$

where ρ_f is the fluid density and $\vec{v}$ its velocity. For an incompressible fluid, this equation takes the following form:

$$\frac{\partial v_x}{\partial x} + \frac{\partial v_y}{\partial y} + \frac{\partial v_z}{\partial z} = 0 \tag{2}$$

where v_x, v_y, and v_z are the components of the velocity vector in the directions of the coordinate system axes (Figure 1).

The general form of the Navier–Stokes equation resulting from momentum balance is as follows:

$$\rho \left(\frac{\partial \vec{v}}{\partial t} + \left(\vec{v} \cdot \nabla \right) \cdot \vec{v} \right) = -\nabla p + \nabla \cdot \left(\mu \left(\nabla \vec{v} + \left(\nabla \vec{v} \right)^T - \frac{2}{3} \left(\nabla \cdot \vec{v} \right) \overleftrightarrow{I} \right) \right) + \rho \vec{g} \tag{3}$$

where ρ_f, $\vec{v}$, p, μ, $\overleftrightarrow{I}$, and $\vec{g}$ are the fluid density, velocity, pressure, dynamic viscosity, identity tensor, and gravity vector, respectively. Assumptions of steady flow, incompressible fluid, and no gravitational force allow us to simplify Equation (3) to the form:

$$\begin{aligned}
\rho_f \left(v_x \frac{\partial v_x}{\partial x} + v_y \frac{\partial v_x}{\partial y} + v_z \frac{\partial v_x}{\partial z} \right) &= -\frac{\partial p}{\partial x} + \left(\frac{\partial}{\partial x} \left(\mu \frac{\partial v_x}{\partial x} \right) + \frac{\partial}{\partial y} \left(\mu \frac{\partial v_x}{\partial y} \right) + \frac{\partial}{\partial z} \left(\mu \frac{\partial v_x}{\partial z} \right) \right) \\
\rho_f \left(v_x \frac{\partial v_y}{\partial x} + v_y \frac{\partial v_y}{\partial y} + v_z \frac{\partial v_y}{\partial z} \right) &= -\frac{\partial p}{\partial y} + \left(\frac{\partial}{\partial x} \left(\mu \frac{\partial v_y}{\partial x} \right) + \frac{\partial}{\partial y} \left(\mu \frac{\partial v_y}{\partial y} \right) + \frac{\partial}{\partial z} \left(\mu \frac{\partial v_y}{\partial z} \right) \right) \\
\rho_f \left(v_x \frac{\partial v_z}{\partial x} + v_y \frac{\partial v_z}{\partial y} + v_z \frac{\partial v_z}{\partial z} \right) &= -\frac{\partial p}{\partial z} + \left(\frac{\partial}{\partial x} \left(\mu \frac{\partial v_z}{\partial x} \right) + \frac{\partial}{\partial y} \left(\mu \frac{\partial v_z}{\partial y} \right) + \frac{\partial}{\partial z} \left(\mu \frac{\partial v_z}{\partial z} \right) \right)
\end{aligned} \tag{4}$$

where ρ_f, p, and μ are the density, pressure, and viscosity of the fluid, respectively.

The general heat transfer equation of the single-phase medium resulting from energy balance is:

$$\rho c_p \left(\frac{\partial T}{\partial t} + \vec{v} \cdot \nabla T \right) = \nabla \cdot (\lambda \nabla T) + \overleftrightarrow{\sigma} \cdot \overleftrightarrow{d} + \rho r \tag{5}$$

where c_p, T, $\vec{v}$, λ, $\overleftrightarrow{\sigma}$, $\overleftrightarrow{d}$, and r are the specific heat capacity, temperature, velocity, thermal conductivity, stress tensor, strain rate tensor, and heat source, respectively.

As a result of the assumptions, the general equation of heat transfer takes the form of an equation for a fluid:

$$\rho_f c_{pf} \left(v_x \frac{\partial T_f}{\partial x} + v_y \frac{\partial T_f}{\partial y} + v_z \frac{\partial T_f}{\partial z} \right) = \lambda_f \left(\frac{\partial^2 T_f}{\partial x^2} + \frac{\partial^2 T_f}{\partial y^2} + \frac{\partial^2 T_f}{\partial z^2} \right) \tag{6}$$

where ρ_f, c_{pf}, T_f, and λ_f are the density, specific heat capacity, temperature, and thermal conductivity of the fluid, respectively.

Since a solid is nondeformable, the only equation that describes its behavior is the heat transfer equation. For a solid, the general Equation (5), after using the assumptions of the model, is simplified to the Laplace equation:

$$\lambda_s \left(\frac{\partial^2 T_s}{\partial x^2} + \frac{\partial^2 T_s}{\partial y^2} + \frac{\partial^2 T_s}{\partial z^2} \right) = 0 \tag{7}$$

where T_s and λ_s are the temperature and thermal conductivity of the solid, respectively.

The final system of equations describing the problem consists of the continuity Equation (2), Navier–Stokes Equation (4), and heat transport Equations (6) and (7). These differential equations require appropriate boundary conditions.

At the inlet to the microchannel, the velocity is assumed to be uniform, perpendicular to the surface, and pressure is also uniform:

$$v_x|_{z=0} = v_y|_{z=0} = 0 \quad v_z|_{z=0} = v_0 \quad p|_{z=0} = p_0 \tag{8}$$

where v_0 and p_0 are the inlet fluid velocity and pressure, respectively.

Due to the viscosity of the fluid, the velocity of the fluid in contact with the solid is assumed to be zero:

$$v_x|_{sl} = 0 \quad v_y|_{sl} = 0 \quad v_z|_{sl} = 0 \tag{9}$$

where index *sl* is the surface between the solid and fluid (solid–liquid interface).

The temperature of the inlet fluid is assumed to be uniform, and the temperature of at the bottom of solid is also assumed to be constant:

$$T_f\Big|_{z=0} = T_{f0} \quad T_s|_{y=0} = T_{s0} \tag{10}$$

where T_{f0} and T_{s0} are the two constant temperatures of fluid and solid, respectively.

Heat transfer between a solid and a fluid occurs through conduction, which means that the heat fluxes described by Fourier's law are equal at the solid–liquid interface:

$$\lambda_s \frac{\partial T_s}{\partial n}\bigg|_{sl} = \lambda_f \frac{\partial T_f}{\partial n}\bigg|_{sl} \tag{11}$$

At both ends of the segment and at the boundary between two adjacent segments, no heat conduction is assumed for the solid body and no heat conduction in the fluid and the end of the segment:

$$\frac{\partial T_s}{\partial z}\bigg|_{z=0} = \frac{\partial T_s}{\partial z}\bigg|_{z=l} = \frac{\partial T_s}{\partial n}\bigg|_{ss} = \frac{\partial T_f}{\partial z}\bigg|_{z=l} \tag{12}$$

where index *ss* means the boundary between solid and solid (two adjacent segments).

$$\text{In the upper part of the region, the conditions of symmetry are assumed,}$$
$$\text{i.e., } \frac{\partial v_x}{\partial y}\bigg|_{y=h} = \frac{\partial v_y}{\partial y}\bigg|_{y=h} = \frac{\partial v_z}{\partial y}\bigg|_{y=h} = 0 \quad \frac{\partial p}{\partial y}\bigg|_{y=h} = 0 \quad \frac{\partial T_f}{\partial y}\bigg|_{y=h} = \frac{\partial T_s}{\partial y}\bigg|_{y=h} = 0 \tag{13}$$

2.4. Method of Solution

The finite volume method (FVM) was used for calculations in this work by Ansys/Fluent implementation. Generally, the method discretizes the computational domain into a set of volumetric cells, that is, control volumes. The governing equations are solved within each control volume, and in a typical scenario the solution is obtained by solving a set of algebraic equations that involve the values of the physical quantities (e.g., pressure, velocity, density, etc.) at the center and/or boundaries of the control volume. The values of the physical quantities are then collected to obtain a solution at any point in the computational domain. The calculation procedure is iterative by design and conver-

gence is controlled by the under-relaxation terms for each equation, which consequently control the advancement process in the solution from one iteration to the next. Additionally, the convergence also depends on the order of the discretization selected for each solved equation.

The geometry of all cases presented was developed using the construction of a solid along a given forming path shaped in the form of an appropriate zigzag. A zigzag profile was inserted into a rectangular area measuring 80 × 9 mm, making the number of sections change from a straight channel with 0 sections to 7, then to 10, and finally to 16 sections. The cooling channel was shaped from a rectangular profile with dimensions of 1 × 0.5 mm.

The size of the tetrahedral mesh cells was determined by the classical procedure based on a series of calculations with changing the base size of the cell. As soon as the mesh size decreased, no significant changes were observed in the obtained mass imbalance, taken as the difference between input and output; the base size of the mesh cells was considered sufficiently small to realistically express the running process. The figure below (Figure 3) presents the convergent profile of results against mesh size. As a size that guarantees the correct accuracy of the calculations with a reasonable calculation rate, 10^{-4} m was selected.

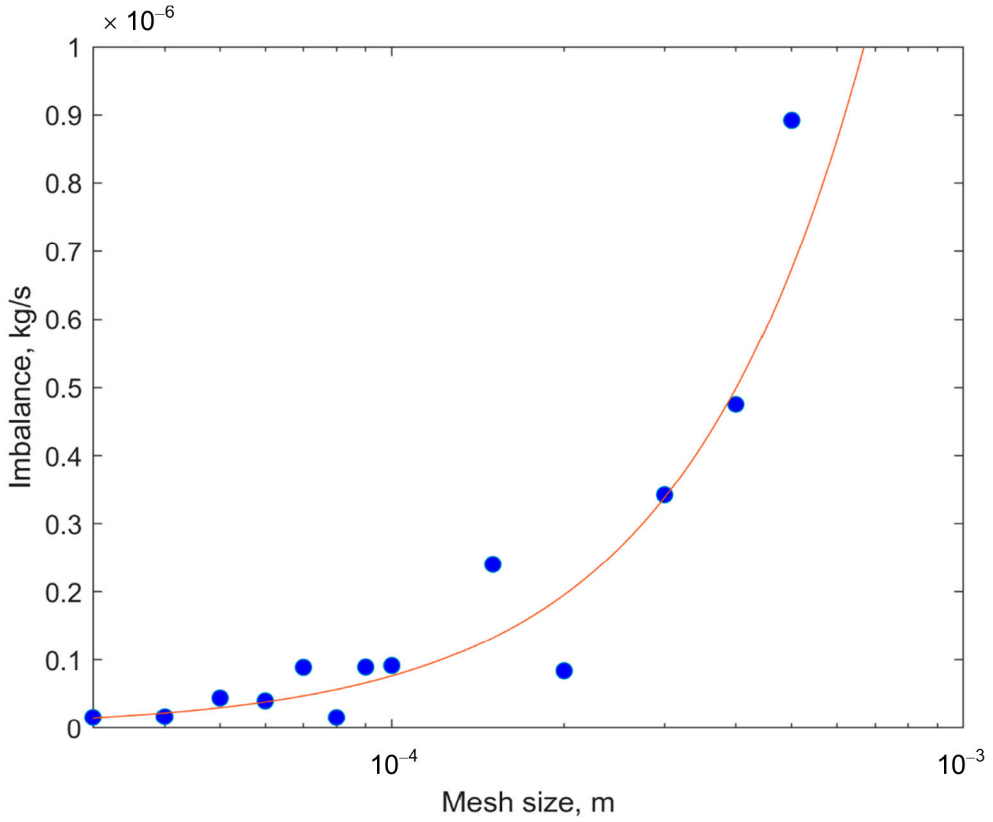


Figure 3. Solution imbalance vs. size of the tetrahedral cell. An improved convergence with reducing mesh size can be observed. The blue dots indicate numerical values and the line show the trend of convergence.

The flow problem was solved using a pressure-velocity coupling scheme (in which pressures and velocities are updated simultaneously). The gradients required for the calculations were defined by a least squares cell-based scheme. The pressure was discretized using second order and the momentum and energy using second order upwind scheme. The coupled approach presents several advantages over the noncoupled or segregated approach. It yields a robust and efficient single-phase implementation for steady-state flows, demonstrating superior performance compared to the segregated solution schemes. The pressure-based coupled algorithm offers an alternative to the density-based and pressure-based segregated algorithms with SIMPLE-type pressure-velocity coupling. In the case of

transient flows (which were not calculated here), employing the coupled algorithm becomes necessary when either the mesh quality is poor or large time steps are employed. The coupled algorithm simultaneously solves the momentum- and pressure-based continuity equations. Full implicit coupling is achieved through an implicit discretization of pressure gradient terms in the momentum equations and an implicit discretization of the face mass flux, incorporating Rhie–Chow pressure dissipation terms. The Rhie–Chow pressure dissipation terms involve the introduction of an extra term to the pressure equation that depends on the velocity field. This term, known as the pressure correction term, acts to dissipate pressure fluctuations that are not consistent with the velocity field, thereby improving the stability of the simulation. The pressure correction term is proportional to the difference between the actual pressure gradient at the face, which is computed based on the velocity field in the adjacent cells and the pressure gradient that would be obtained by interpolating the pressure values from the neighboring cells. This approach allows for a more accurate calculation of the pressure and velocity fields and ensures that they were in appropriate agreement. Such a methodology provided reliable solutions to the flow simulation tasks selected in this work.

2.5. Applied Materials

In microchannels, water or nanofluids are usually used as the coolant. Sakanova and co-workers [27] analyzed water and three nanofluids as coolant in wavy channels. They found that the use of nanofluids in curved microchannels is not appropriate. Therefore, water is chosen as the coolant in the present analysis. Aluminum was chosen as the material in which the microchannels are made because it is a material with high thermal conductivity and corrosion resistance. The water and aluminum materials coefficients are given in Table 2.

Table 2. The properties of the components used in the calculations.

Property	Water	Aluminum
Density, kg/m^3	DIPPR 105 (Equation (15))	2719
Viscosity, kg/m·s	DIPPR 101 (Equation (14))	
Specific heat, J/kg·K	4182	871
Thermal conductivity, W/m·K	0.6	202.4

In Table 2, references are made to the DIPPR equations, which are defined in the DIPPR-801 project, released in the early 1980s by the Design Institute for Physical Properties (DIPPR, New York, NY, USA) to describe the temperature dependence of various important physical properties of substances [34]. They are the industry standard in many applications where substance data are needed for optimizing and designing chemical processes as well as in process synthesis, simulations, and development. The DIPPR-801 database contains parameter sets for about 2000 substances. The equations have proven to be highly reliable and accurate in predicting the temperature dependence of various thermophysical properties.

According to DIPPR, the water viscosity (14) and density (15) can be calculated using the following correlations:

– viscosity.

$$\eta = \exp\left(A + B\frac{1}{T} + C \cdot \ln(T) + D \cdot T^E\right) \quad (14)$$

– density.

$$\rho = A \cdot B^{-(1+(1-\frac{T}{C})^D)} \cdot M_{mol} \quad (15)$$

In the above, the corresponding constants were taken for water from the DIPPR database. M_{mol} is molar mass and is used to recalculate the molar to mass density. Table 3 presents values for both correlations.

Table 3. The coefficients values for properties temperature correlations [34].

Property	A	B	C	D	E
Viscosity, Pa·s	−51.964	3670.6	5.7331	-5.3495×10^{-29}	10
Density, kmol/m^3	5.459	0.30542	647.13	0.081	-

2.6. Considered Cases

The simulations were conducted to investigate the effects of two process data, namely inlet velocity and temperature of the hot bottom face, on the thermal performance of four distinct geometries. It was assumed that the cooling water entered the channel at a temperature of 292 K. To examine the impact of the inlet flow on the system, a range of values was defined between 0.1 m/s and 0.8 m/s with a step of 0.1 m/s for the inlet velocity. Furthermore, the temperature of the bottom hot surface varied from 330 K to 360 K with a step change of 10 K.

A total of 32 simulation calculations were performed for each of the four cases, resulting in a total of 128 simulation runs. Simulations were performed using described earlier computational techniques and algorithms to accurately model and predict the behavior of the system. The results obtained from the simulations were analyzed using post-processing methods to obtain insights into the thermal performance of the geometries under different process conditions.

2.7. Analyzed Parameters

This section presents formulas used to calculate the values of parameters characterizing the quality of liquid flow in microchannels and the quality of heat exchange between a solid and a liquid.

The first parameter is the difference in the mean pressure at the inlet and outlet of the microchannel (pressure drop):

$$\Delta p = p|_{y=0} - p|_{z=l} = p_0 - p|_{z=l} \tag{16}$$

where the average outlet pressure is:

$$p|_{z=l} = \frac{1}{A_f} \iint\limits_{A_f} p \, dxdy \Bigg|_{z=l} \tag{17}$$

and $A_f = a \times c$ is the microchannel cross-section. The power needed to force the flow of a given intensity is:

$$P = p_0 v_0 A_f - \iint\limits_{A_f} pv \, dxdy \Bigg|_{z=l} \tag{18}$$

The value of the pressure drop in the microchannels is determined by the Darcy–Weisbach equation:

$$\Delta p = f \frac{l}{D_h} \frac{\rho_f v_0^2}{2} \tag{19}$$

where for a square section the hydraulic diameter is $D_h = a$. Rearranging Equation (19) gives the Darcy friction factor f:

$$f = \frac{2a\Delta p}{\rho_f v_0^2 l} \tag{20}$$

The Darcy friction coefficient is a metric of flow resistance. It offers insights that can be leveraged to optimize flow systems, thereby minimizing pressure losses and enhancing the overall efficiency of equipment.

The heat flux carried away by the fluid results from the difference between the outgoing and supplied streams:

$$\dot{Q} = \iint\limits_{A_f} \rho_f v_z c_{pf} T_f \, dxdy \Bigg|_{z=l} - \left(\rho_f c_{pf}\right)_{z=0} v_0 T_{f0} A \tag{21}$$

This heat flux is the most important parameter that describes the cooling effect of the microchannel.

The volumetric average fluid temperature is:

$$\overline{T}_f = \frac{1}{V_f} \iiint\limits_{V_f} T_f(x,y,z) dV \tag{22}$$

while the average temperature of the surface separating the liquid and the solid is:

$$\overline{T}_{sl} = \frac{1}{A_{sl}} \iint\limits_{A_{sl}} T_s(x,y,z) dA \tag{23}$$

The heat flux received from the cooled element, equal to the heat flux carried away by the fluid, is described by the Newton equation:

$$\dot{Q} = \alpha A \Delta T \tag{24}$$

where α is the average heat transfer coefficient. This coefficient can be calculated by assuming that the temperature difference concerns the average values:

$$\Delta T = \overline{T}_{sl} - \overline{T}_f \tag{25}$$

and the solid–liquid interface of a simple microchannel is taken as the heat transfer surface (reference surface):

$$A = (a + 2h)l \tag{26}$$

In this case, the average heat transfer coefficient α is:

$$\alpha = \frac{\dot{Q}}{(a + 2h)l\left(\overline{T}_{sl} - \overline{T}_f\right)} \tag{27}$$

Based on knowledge of the average heat transfer coefficient, the average value of the Nusselt number can be calculated:

$$\mathrm{Nu} = \frac{\alpha D_h}{\lambda_f} \tag{28}$$

The Nusselt number describes the quality of convective heat transfer in a dimensionless way. It is used in practice in the design of all types of heat exchangers.

To assess the quality of operation of microchannels of various shapes, working under different flow conditions and in different temperature ranges, the quality factor can be introduced, which is the ratio of the total heat transfer rate during cooling to the power needed to force the flow:

$$\eta = \frac{\dot{Q}}{P} \tag{29}$$

3. Results

In this work, we focus on simulations of heat transport in microchannels to study the behavior of this process and to investigate the effects of various design parameters on overall system performance. In this chapter, we present the results of our simulations, including the key observations and trends we identified, as well as the implications of our results for potential applications in various fields.

Figure 4 presents streamlines for the most complex shape calculated, the channel with segment number n = 16. At the location where the streamline encounters a change in direction, such as a bend or, in this case, a corner, the fluid may experience local reversed flow due to the differences in fluid velocity and pressure between the inner and outer walls of the bend. This can cause the fluid to separate from the wall and form eddies, which can be seen in the calculated streamline as regions where the flow direction changes abruptly or where the streamline curves back on itself. The size and shape of the eddies depend on factors such as the curvature of the bend, the speed of the fluid, and the viscosity of the fluid.

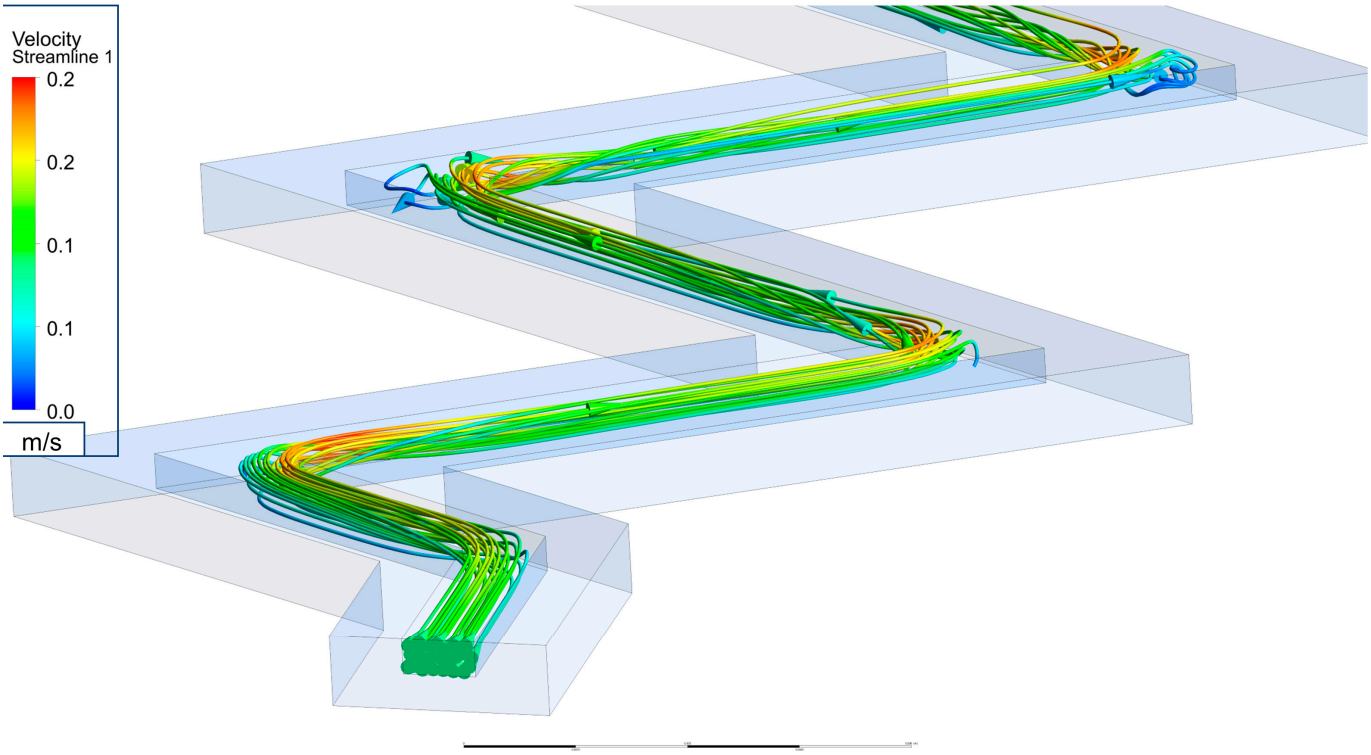


Figure 4. Streamlines for channel n = 16.

One of the significant flow parameters is the pressure drop, presented in Figure 5. The calculated data presented suggested that as the inlet velocity increases, there is an increase in pressure drop across the microchannel, which is consistent with the principle of fluid mechanics that the pressure drop in a channel is directly proportional to the velocity of the fluid. Additionally, while the data indicate that an increase in the bottom temperature of the microchannel corresponds to a decrease in pressure drop, this effect appears to be marginal when compared to the more pronounced influence of fluid velocity on the pressure dynamics within the microchannel. This implies that the thermal properties of the fluid and the channel have an important impact on the pressure drop. Furthermore, the data suggest that the effect of inlet velocity on the pressure drop is more pronounced than the effect of the bottom temperature. The more complex the shape of the channel, the higher is the pressure drop, again as expected by fluid flow principles.

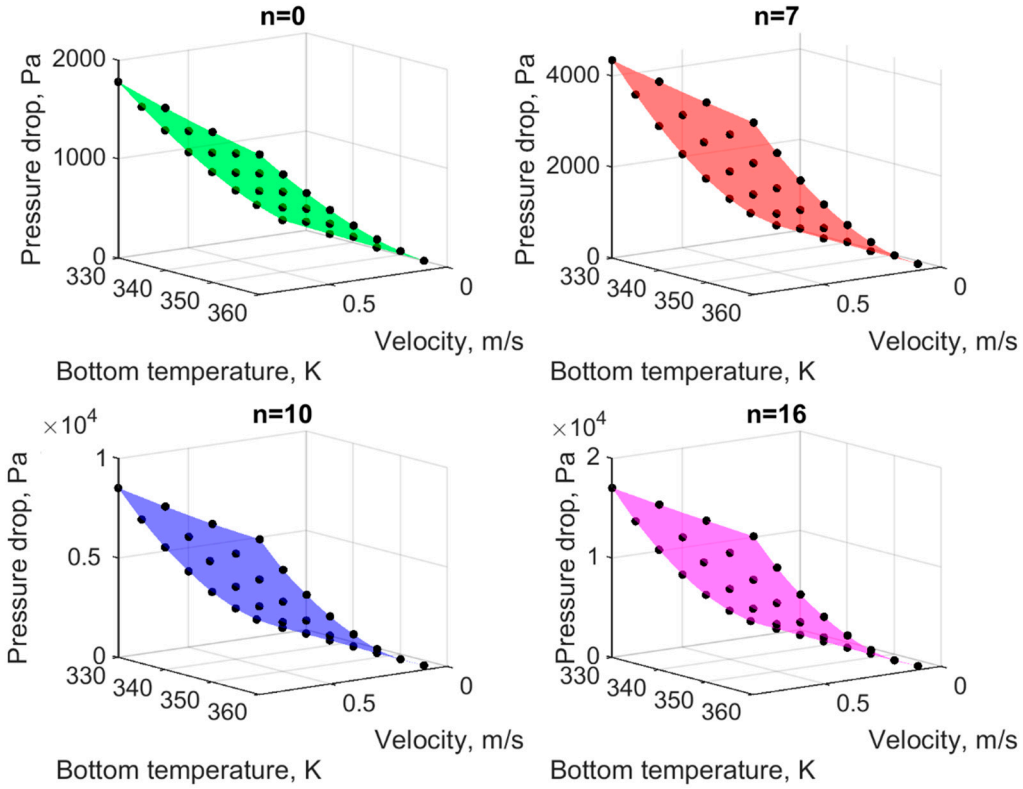


Figure 5. Pressure drop.

The results presented in Figure 6 show that the hydraulic power in the microchannel is a function of both the inlet velocity and the bottom temperature. As the inlet velocity increases, the hydraulic power also increases, which is expected, as higher velocity results in greater fluid flow. On the contrary, as the bottom temperature increases, the hydraulic power decreases, which is related to the decrease in viscosity and density of the fluid. It can also be observed that higher velocities lead to an increased rate of rise in hydraulic power, although the effect of temperature on this increase is relatively marginal. The more complex the channel design, the more power that is required also increases. These results can provide insight into the optimization of microchannel heat transfer systems, such as determining the appropriate flow and temperature conditions to predict the required hydraulic power levels.

The Darcy friction factor is presented in Figure 7, showing that its value decreases as the inlet velocity increases, while the effect of increasing heating bottom temperature is observed to be comparatively marginal. This result illustrates the fact that there is an intermediate relationship between the heating temperature and resistance. It can be seen that higher velocities lead to a decreased resistance to flow through the microchannel. It is also noticeable that the effect of the inlet velocity on the Darcy coefficient is more significant than the effect of the heating bottom temperature. This can be observed by comparing the values of the Darcy coefficient for different inlet velocities at the same heating bottom temperature. Also, it is visible that a higher number of zigzags results in higher friction factor values.

Figure 8 shows the water temperature distributions in the microchannels for the bottom temperature $T_{s0} = 360$ K and the inlet velocity $v_0 = 0.1$ m/s. The temperature increases along the flow. It is clearly visible that increasing the number of zigzag pattern segments improves the heat exchange between the solid and the water flowing inside the microchannel. Each bend of the microchannel causes the flowing water to mix (Figure 4), resulting in improved heat transfer.

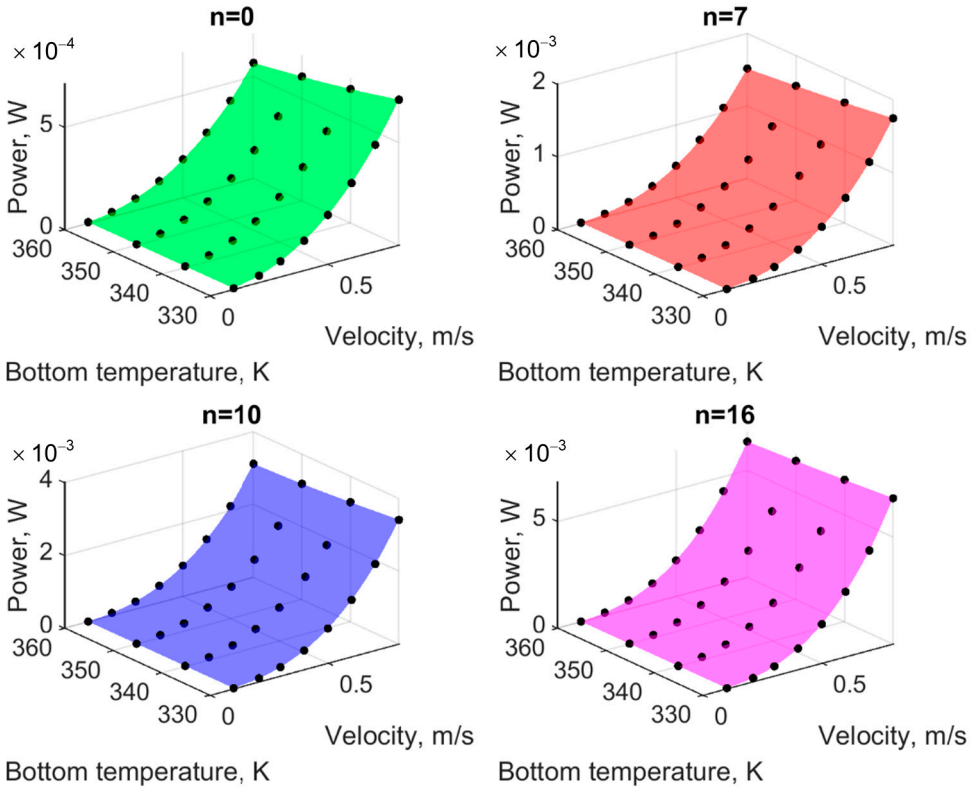


Figure 6. Power, P, used to force the flow.

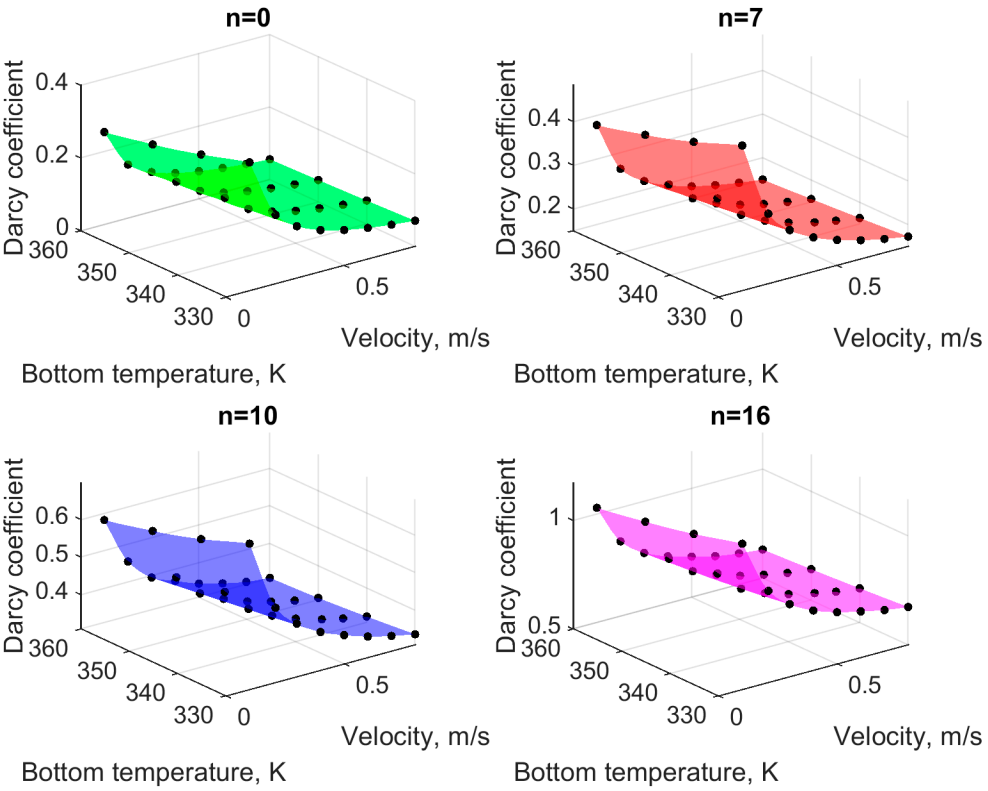


Figure 7. Darcy friction factor, f.

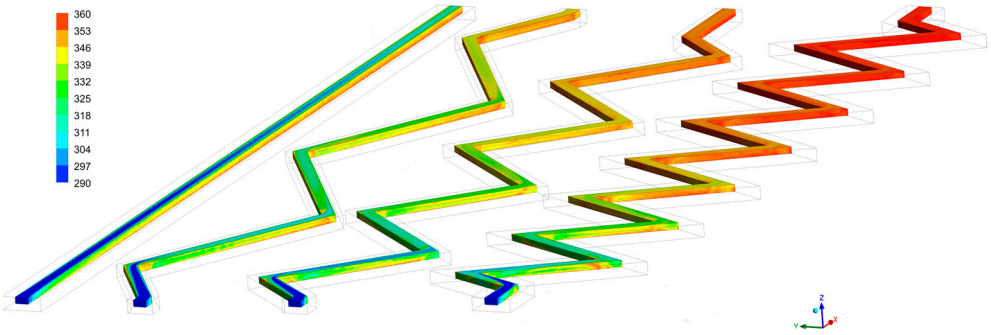


Figure 8. Temperature distribution along the microchannels for bottom temperature at 360 K and inlet velocity 0.1 m/s.

Figure 9 shows the average temperature of the outlet water for all considered cases. For all microchannels, increasing the bottom temperature, T_{s0}, increases the outlet temperature. Increasing the flow rate in a straight microchannel significantly reduces the outlet temperature of the fluid. However, this effect becomes more pronounced with the introduction of zigzag bends; for higher flow velocities, the outlet temperature notably increases. While this trend holds true across all cases, it is especially evident in microchannels with zigzag shapes, where the influence of the number of zigzag segments on the outlet temperature is more marked.

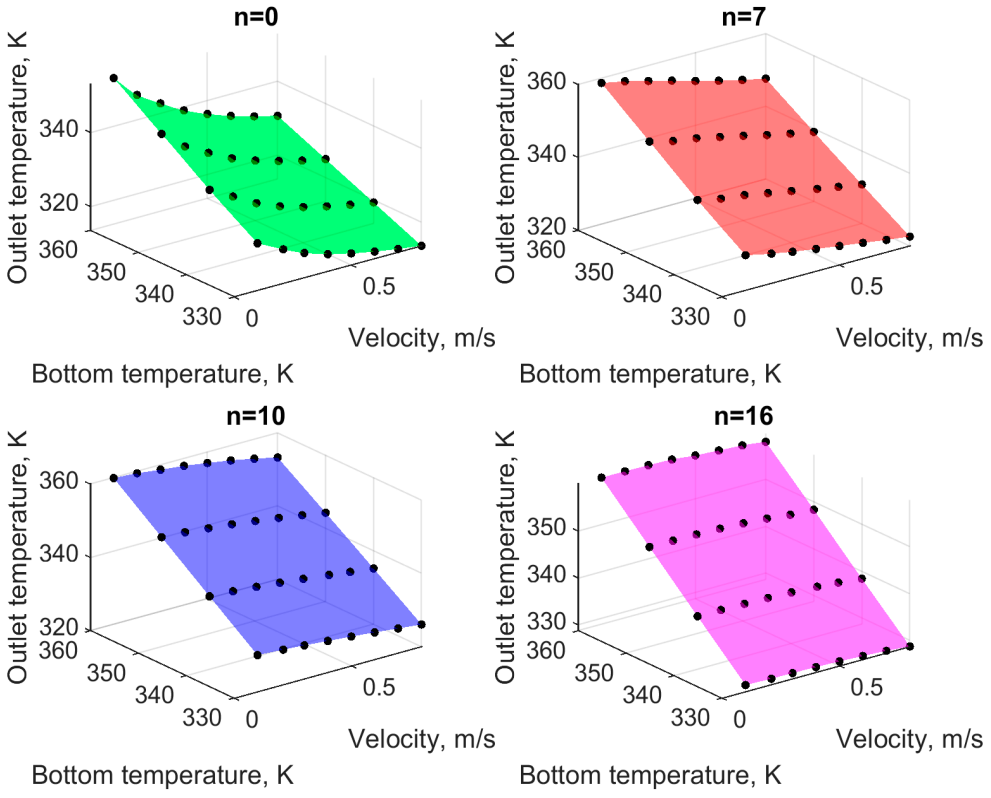


Figure 9. Average outlet fluid temperature, T_f.

Figure 10 shows the heat flux carried away by the fluid, $\dot{Q}$, (Equation (21)) for all considered cases. When the flow velocity is low, the differences in heat transfer between the various microchannel shapes are not substantial. The total heat transfer is understandably dependent on the bottom temperature, T_{s0}. However, at higher flow velocities, the number of zigzag segments increasingly affects the amount of heat transferred. Enhancing the number of these segments has been shown to improve the microchannel's heat dissipation capability.

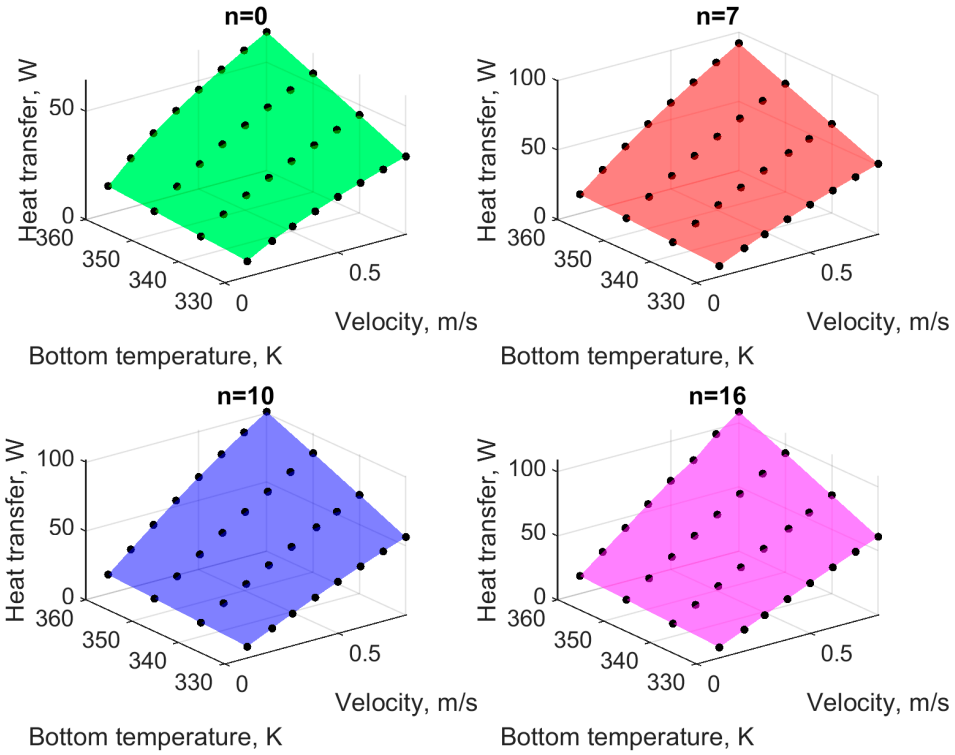


Figure 10. Heat flux, $\dot{Q}$.

Figure 11 shows the averaged heat transfer coefficient, α, (Equation (27)) for all considered cases. As you can see, this coefficient practically does not depend on the bottom temperature, T_{s0}. However, an increase in flow velocity results in an almost linear increase in the coefficient for all microchannels. The greater the number of microchannel segments, the greater the increase in the heat transfer coefficient.

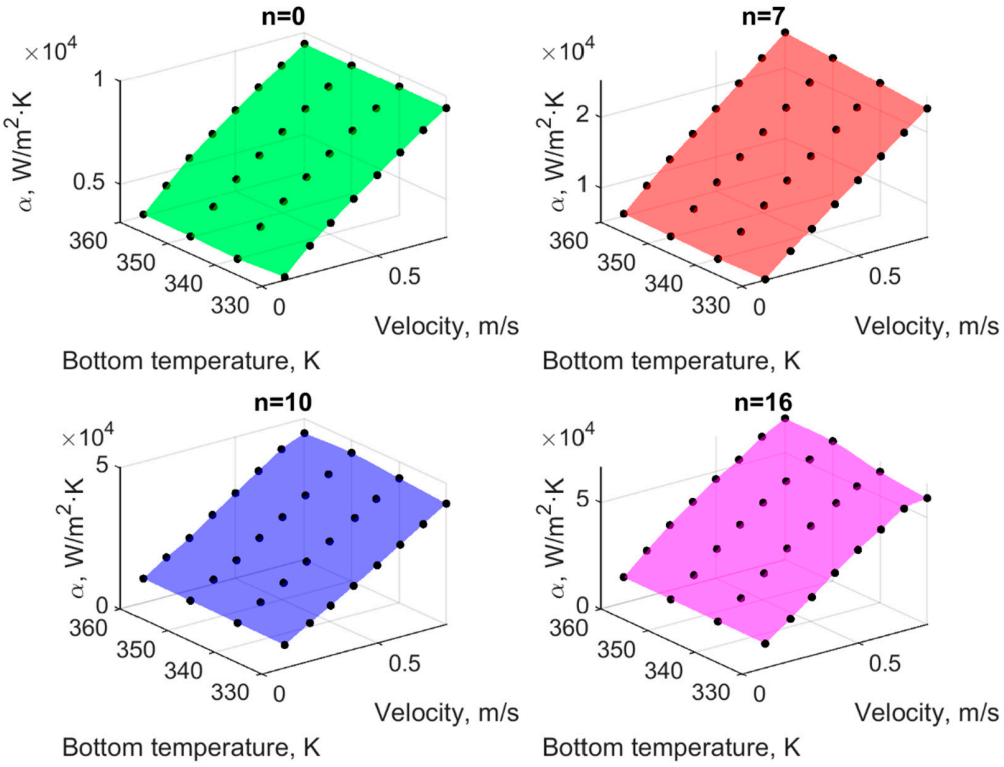


Figure 11. Averaged heat transfer coefficient, α.

Heat transfer from a solid to a fluid can also be described by the dimensionless Nusselt number (Equation (28)). The Nusselt number shown in Figure 12 has exactly the same properties as the heat transfer coefficient, i.e., it does not depend on the temperature, but it varies with the flow velocity and the number of zigzag segments. The obtained values of Nusselt number are several times higher compared to those obtained experimentally by Gaikwad and Nalawade [Gaikwad]. This is due to the greater amplitude of the grooves compared to [Gaikwad] as well as the greater number of zigzags. These geometric differences result in increased flow disturbance and consequently, improved heat transfer. It should be noted that the flow velocity has a large influence on heat transfer. The Nusselt number changes several times with the increase in flow velocity. This type of effect was observed, among others, by Sui et al. [26].

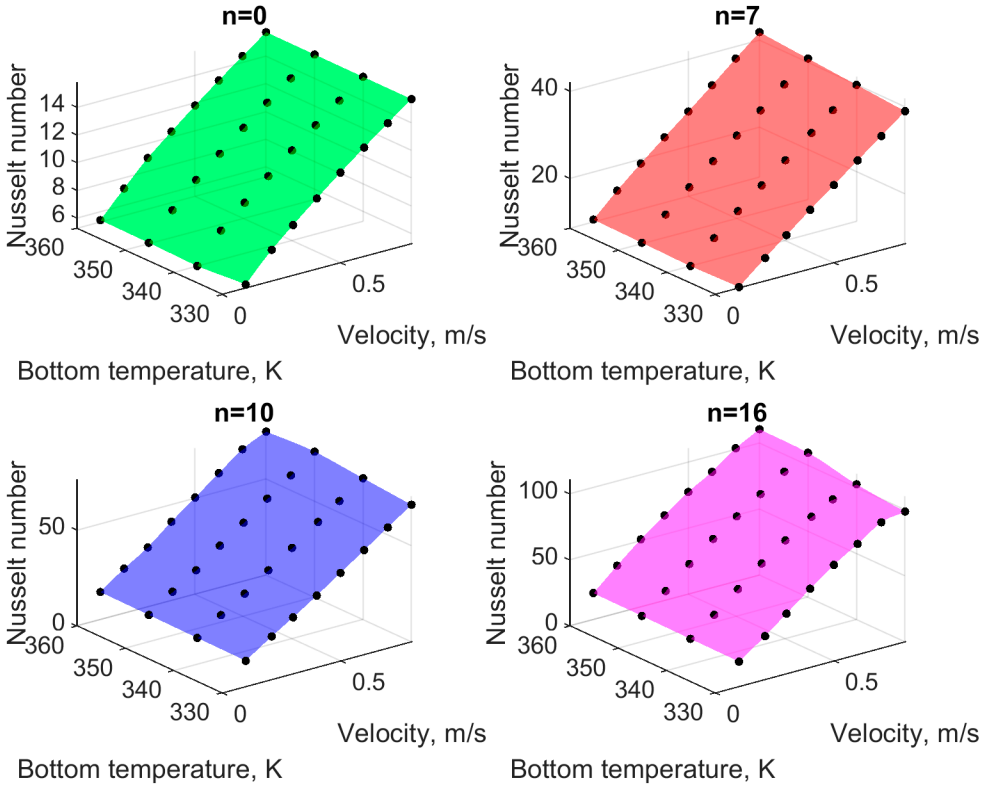


Figure 12. Nusselt number, Nu.

Figure 13 shows the quality factor, η. This factor is the ratio of the heat flux during cooling to the power needed to force the flow (Equation (29)). The higher the value of the coefficient, the better the performance of the microchannel from the point of view of comparing the energy taken out in the form of heat with the energy used to forcing the flow. The coefficient values for all cases are greater than 10^5, which means that the energy needed to force the flow is negligibly small compared to the heat released. So, all microchannels perform a cooling function well.

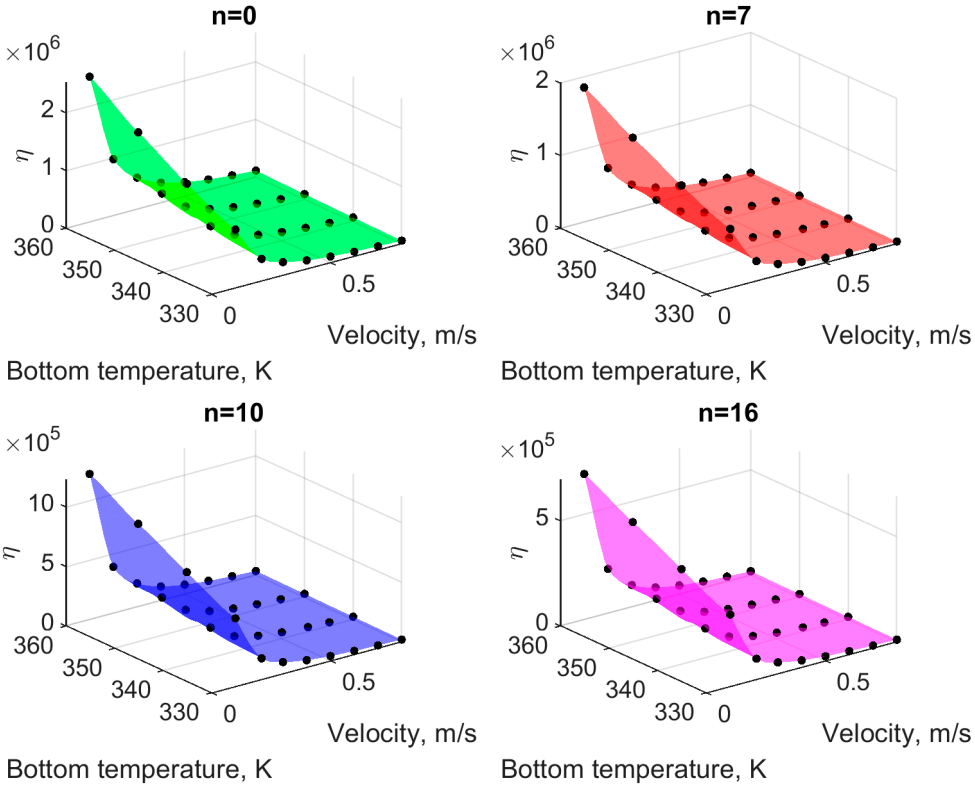


Figure 13. Quality factor η.

4. Discussion

In this work, fluid flow and heat transfer in a zigzag-shaped microchannel were studied. The results of all simulations showed that the use of a non-rectilinear shape increases the pressure drop along the microchannel (Figure 5) and, thus, increases the flow resistance. This is in line with the results presented in [28–31]. The increase in the length of the flow path and disturbances in the velocity distribution, such as flow separation, local flow reversal, or induced flows, jointly contribute to this phenomenon. These effects are synergistically responsible for the observed behaviors and are visibly illustrated in Figure 4, which displays the streamlines. The increase in flow resistance due to the shape of the microchannel increases the demand for power needed to force the flow (Figure 6) and increases the Darcy coefficient of friction (Figure 7). Studies have shown that the greater the number of zigzag sections, the greater the flow resistance (Figures 5–7).

The influence of flow velocity through the microchannels was investigated. As expected, the higher the speed, the greater the pressure drop (Figure 5) and the greater the power required to force the flow (Figure 6). Increasing the flow rate also results in a decrease in the Darcy coefficient of friction (Figure 7). These results also coincide with the results presented in [28–31].

Our study also investigated the influence of the temperature of the heat source on the flow of the coolant. All the results (Figures 5–7) indicate a trend where increasing the temperature of the heat source reduces the flow resistance. This phenomenon results from the fact that increasing the temperature causes a decrease in the viscosity coefficient (Equation (14)), which in turn, marginally reduces the friction resistance. It is important to note, however, that the relative impact of temperature on flow resistance appears to be minor. This aspect of our findings is not readily comparable with existing literature, which typically presumes a constant heat flux density from the heat source, hence the specific effect of temperature on flow resistance has not been extensively explored to date.

Studies have shown that the use of non-rectilinear microchannels improves heat transfer. This is also in line with the results of works [28–33]. It is obvious that the temperature of the coolant increases along the flow. In addition, each bend of the microchannel causes

mixing of the liquid, resulting in a local improvement in heat exchange (Figure 8). As a result, each increase in the number of zigzag segments results in an increase in the outlet fluid temperature (Figure 9). However, it should be noted that the higher the number of these segments, the smaller the change in the outlet temperature. The influence of the flow rate of the cooling liquid on the outlet temperature is also clear. The higher the speed, the lower the temperature. This is especially evident for the straight microchannel (Figure 9).

The outlet temperature and flow rate are the main parameters that affect the heat carried away by the fluid. As the results of numerical simulations show (Figure 10), this heat transfer and hence cooling performance increases with the outlet temperature. Although this temperature decreases with increasing flow velocity (Figure 9); however, increasing the velocity increases this heat flux (Figure 10). It is worth emphasizing that while the addition of zigzag segments initially enhances heat transfer performance, the degree of improvement diminishes as the number of segments increases.

The heat exchange between a fluid and a solid is described by two parameters: the dimensional heat transfer coefficient and the dimensionless Nusselt number. Their values are presented in Figures 11 and 12. As can be seen, they are practically independent of the temperature of the heat source and, consequently, of the temperature of the fluid. However, it is clear that increasing the flow velocity increases both of these factors. These results are in line with the results taken from the literature [28–31]. Increasing the flow velocity reduces the thickness of the boundary layer. In turn, increasing the number of zigzag segments results in local mixing of the cooling liquid. This has a great influence on heat transfer. The result is an increase in the heat transfer coefficient and the Nusselt number.

Further research on heat transfer using flows in microchannels should proceed in two directions. First, calculations should be made for flows in various geometries, assuming that the temperature of the heating element is known (so far, a known heat flux has been considered). Second, these calculations should continue to check the effect of using special cooling fluids other than water.

5. Conclusions

The results of numerical simulations presented in the paper clearly indicate that the use of non-rectilinear microchannels as heat sinks is an efficient method of cooling. The additional flow resistance generated by the non-linear shape of the microchannels is negligibly small with improved heat transfer. Each increase in the number of zigzag segments improves the cooling capacity. The higher the flow rate of the cooling liquid, the greater the influence of the zigzag segments used. However, it should be noted that the increase in heat transfer decreases with the increase in the number of these segments. Therefore, when designing such elements, their shape and number should be adapted to specific conditions.

Author Contributions: Conceptualization, G.M. and M.S.; methodology, G.M. and M.S.; software, M.S.; validation, G.M. and M.S.; writing—original draft preparation G.M. and M.S.; writing—review and editing, G.M. and M.S.; visualization, M.S.; supervision, G.M. and M.S.; project administration, G.M. and M.S.; All authors have read and agreed to the published version of the manuscript.

Funding: This research was funded by Ministry of Science and Higher Education, Poland.

Data Availability Statement: The data presented in this study are available on request from the corresponding author. The data are not publicly available due to privacy.

Conflicts of Interest: The authors declare no conflicts of interest.

References

1. Zhang, Z.; Wang, X.; Yan, Y. A review of the state-of-the-art in electronic cooling. *e-Prime Adv. Electr. Eng. Electron. Energy* **2021**, *1*, 100009. [CrossRef]
2. Kandlikar, S.G.; Bapat, A.V. Evaluation of Jet Impingement, Spray and Microchannel Chip Cooling Options for High Heat Flux Removal. *Heat Transf. Eng.* **2007**, *28*, 911–923. [CrossRef]
3. Tong, H.H.; Lai, Y.-S.; Wong, C.P. (Eds.) *Advanced Flip Chip Packaging*; Springer: New York, NY, USA; London, UK, 2010.

4. Sohel Murshed, S.M.; Nieto de Castro, C.A. A critical review of traditional and emerging techniques and fluids for electronics cooling. *Renew. Sustain. Energy Rev.* **2017**, *78*, 821–833. [CrossRef]
5. El Alami, M.; Najam, M.; Semma, E.; Oubarra, A.; Penot, F. Electronic components cooling by natural convection in horizontal channel with slots. *Energy Convers. Manag.* **2005**, *46*, 2762–2772. [CrossRef]
6. Kuncoro, I.W.; Pambudi, N.A.; Biddinika, M.K.; Widiastuti, I.; Hijriawan, M.; Wibowo, K.M. Immersion cooling as the next technology for data center cooling: A review. *J. Phys. Conf. Ser.* **2019**, *1402*, 044057. [CrossRef]
7. Kim, J. Spray cooling heat transfer: The state of the art. *Int. J. Heat Fluid Flow* **2007**, *28*, 753–767. [CrossRef]
8. Cheng, J.-T.; Chen, C.-L. Active thermal management of on-chip hot spots using EWOD-driven droplet microfluidics. *Exp. Fluids* **2010**, *49*, 1349–1357. [CrossRef]
9. Sabato, M.; Fregni, A.; Stalio, E.; Brusiani, F.; Tranchero, M.; Baritaud, T. Numerical study of submerged impinging jets for power electronics cooling. *Int. J. Heat Mass Transf.* **2019**, *141*, 707–718. [CrossRef]
10. Tang, H.; Tang, Y.; Wan, Z.; Li, J.; Yuan, W.; Lu, L.; Li, Y.; Tang, K. Review of applications and developments of ultra-thin micro heat pipes for electronic cooling. *Appl. Energy* **2018**, *223*, 383–400. [CrossRef]
11. Chen, Z.; Li, Y.; Zhou, W.; Deng, L.; Yan, Y. Design, fabrication and thermal performance of a novel ultra-thin vapour chamber for cooling electronic devices. *Energy Convers. Manag.* **2019**, *187*, 221–231. [CrossRef]
12. Salunkhe, P.B.; Shembekar, P.S. A review on effect of phase change material encapsulation on the thermal performance of a system. *Renew. Sustain. Energy Rev.* **2012**, *16*, 5603–5616. [CrossRef]
13. Tuckerman, D.; Pease, R. High-performance heat sinking for VLSI. *IEEE Electron Device Lett.* **1981**, *2*, 126–129. [CrossRef]
14. Sidik, N.A.C.; Muhamad, M.N.A.W.; Japar, W.M.A.A.; Rasid, Z.A. An overview of passive techniques for heat transfer augmentation in microchannel heat sink. *Int. Commun. Heat Mass Transf.* **2017**, *88*, 74–83. [CrossRef]
15. Abubakar, S.B.; Sidik, N.A.C.; Ahmad, A.S. The use of Fe_3O_4-H_2O_4 Nanofluid for Heat Transfer Enhancement in Rectangular Microchannel Heatsink. *J. Adv. Res. Mater. Sci.* **2016**, *23*, 15–24.
16. Gunnasegaran, P.; Mohammed, H.; Shuaib, N.; Saidur, R. The effect of geometrical parameters on heat transfer characteristics of microchannels heat sink with different shapes. *Int. Commun. Heat Mass Transf.* **2010**, *37*, 1078–1086. [CrossRef]
17. Song, J.; Liu, F.; Sui, Y.; Jing, D. Numerical studies on the hydraulic and thermal performances of trapezoidal microchannel heat sink. *Int. J. Therm. Sci.* **2021**, *161*, 106755. [CrossRef]
18. Hasan, M.I.; Rageb, A.; Yaghoubi, M.; Homayoni, H. Influence of channel geometry on the performance of a counter flow microchannel heat exchanger. *Int. J. Therm. Sci.* **2009**, *48*, 1607–1618. [CrossRef]
19. Ghaedamini, H.; Lee, P.; Teo, C. Developing forced convection in converging–diverging microchannels. *Int. J. Heat Mass Transf.* **2013**, *65*, 491–499. [CrossRef]
20. Wong, K.-C.; Lee, J.-H. Investigation of thermal performance of microchannel heat sink with triangular ribs in the transverse microchambers. *Int. Commun. Heat Mass Transf.* **2015**, *65*, 103–110. [CrossRef]
21. Chai, L.; Xia, G.; Zhou, M.; Li, J.; Qi, J. Optimum thermal design of interrupted microchannel heat sink with rectangular ribs in the transverse microchambers. *Appl. Therm. Eng.* **2013**, *51*, 880–889. [CrossRef]
22. Li, M.; Gao, X.; Li, H.; Sang, J.; Nie, P.; Fang, W.; Xu, T. Investigation of Flow and Heat Transfer Characteristics in Microchannels with Fins. *Machines* **2023**, *11*, 154. [CrossRef]
23. Gaikwad, S.M.; Nalawade, M.K. Investigation of heat transfer and fluid flow characteristics in straight and zigzag microchannels with water as working medium. *Int. J. Ambient Energy* **2022**, *43*, 5006–5012. [CrossRef]
24. Sui, Y.; Teo, C.; Lee, P.; Chew, Y.; Shu, C. Fluid flow and heat transfer in wavy microchannels. *Int. J. Heat Mass Transf.* **2010**, *53*, 2760–2772. [CrossRef]
25. Sui, Y.; Lee, P.; Teo, C. An experimental study of flow friction and heat transfer in wavy microchannels with rectangular cross section. *Int. J. Therm. Sci.* **2011**, *50*, 2473–2482. [CrossRef]
26. Sui, Y.; Teo, C.; Lee, P. Direct numerical simulation of fluid flow and heat transfer in periodic wavy channels with rectangular cross-sections. *Int. J. Heat Mass Transf.* **2011**, *55*, 73–88. [CrossRef]
27. Sakanova, A.; Keian, C.C.; Zhao, J. Performance improvements of microchannel heat sink using wavy channel and nanofluids. *Int. J. Heat Mass Transf.* **2015**, *89*, 59–74. [CrossRef]
28. Zhou, J.; Hatami, M.; Song, D.; Jing, D. Design of microchannel heat sink with wavy channel and its time-efficient optimization with combined RSM and FVM methods. *Int. J. Heat Mass Transf.* **2016**, *103*, 715–724. [CrossRef]
29. Mohammed, H.; Gunnasegaran, P.; Shuaib, N. Numerical simulation of heat transfer enhancement in wavy microchannel heat sink. *Int. Commun. Heat Mass Transf.* **2011**, *38*, 63–68. [CrossRef]
30. Mohammed, H.; Gunnasegaran, P.; Shuaib, N. Influence of channel shape on the thermal and hydraulic performance of microchannel heat sink. *Int. Commun. Heat Mass Transf.* **2011**, *38*, 474–480. [CrossRef]
31. Parlak, Z. Optimal design of wavy microchannel and comparison of heat transfer characteristics with zigzag and straight geometries. *Heat Mass Transf.* **2018**, *54*, 3317–3328. [CrossRef]
32. Pandey, V.K.; Negi, V.P.S.; Ranganayakulu, C. An In-Depth Comparison of Straight and Wavy Microchannel Heat Exchangers. *J. Therm. Sci. Eng. Appl.* **2024**, *16*, 051007. [CrossRef]

33. Li, W.; Yang, F.; Alam, T.; Ren, C. *A Numerical Parametric Study of Flow and Heat Transfer in Circular and Zig-Zag Square Microchannel Heat Sinks*; American Society of Mechanical Engineers Digital Collection: New York, NY, USA, 2016. [CrossRef]
34. DECHEMA | DIPPR 801. Available online: https://dechema.de/en/dippr801.html (accessed on 30 March 2023).

Disclaimer/Publisher's Note: The statements, opinions and data contained in all publications are solely those of the individual author(s) and contributor(s) and not of MDPI and/or the editor(s). MDPI and/or the editor(s) disclaim responsibility for any injury to people or property resulting from any ideas, methods, instructions or products referred to in the content.